Ceramics International 42 (2016) 15889–15896

Contents lists available at ScienceDirect

Ceramics International

journal homepage: www.elsevier.com/locate/ceramint

Enhanced gas sensing properties of hierarchical SnO_2 nanoflower assembled from nanorods via a one-pot template-free hydrothermal method

Qiong Wang*, Na Yao, Dongmin An, Yan Li, Yunling Zou, Xiaoxue Lian, Xiaoqiang Tong

College of Science, Civil Aviation University of China, Tianjin, 300300, China

ARTICLE INFO

Article history:
Received 10 May 2016
Received in revised form
29 June 2016
Accepted 10 July 2016
Available online 12 July 2016

Keywords:
SnO_2
Self-assembly
Hydrothermal synthesis
Nanoflower
Gas sensor

ABSTRACT

Well-defined three-dimensional (3D) hierarchical tin dioxide (SnO_2) nanoflowers with the size of about 200 nm were successfully synthesized by a simple template-free hydrothermal method. X-ray diffraction (XRD), scanning electron microscopy (SEM), transmission electron microscopy (TEM) and N_2 adsorption-desorption analyses were used to characterize the structure and morphology of the products. The as-synthesized full crystalline and large specific surface area SnO_2 nanoflowers were assembled by one-dimensional (1D) SnO_2 nanorods with sharp tips. A possible self-assembly mechanism for the formation the SnO_2 nanoflowers was speculated. Moreover, gas sensing investigation showed the sensor based on SnO_2 nanoflowers to exhibit high response and fast response-recovery ability to detect acetone and ethanol at an operating temperature lower than 200 °C. The enhancement of gas sensing properties was attributed to their 3D hierarchical nanostructure, large specific surface area, and small size of the secondary SnO_2 nanorods.

1. Introduction

One-dimensional nanostructures with their extensive applications in these fields, such as wires, rods, belts and tubes have gained prominent attention due to their unique physical and chemical properties [1–6]. Self-assembly of 1-D functional nanoscale building blocks for preparing 2D or 3D hierarchical structures has also attracted considerable interest [7–11]. Unitl now, the successful applications of various synthetic strategies, including chemical modification [12], electrostatic induction [13], surface-interface interaction [14,15] and template addition [16] for preparing hierarchical structures, such as flowers [14,17], dendrites [18] and urchins [19], have been obtained. However, it is still a challenge to develop complex architectures assembled by 1D nanocrystals by a simple, solution-based, and template-free method.

Tin dioxide (SnO_2), as a wide band n-type semiconductor (E_g=3.6 eV at 300 K), due to its high conductivity, fast response, good stability and low cost, is often applied as a semiconductor-based gas-sensing material for reductive gases such as hydrogen, methane, carbon monoxide, methanol, ethanol and other volatile organic compounds [20–25]. In order to meet the demand for large specific surface area and surface accessibility of analyte molecules, various hierarchical structures of SnO_2 and SnO_2-based composites such as flowers, hollow nanostructures, and mesoporous solids have been synthesized [11,22,25–30]. For gas sensing, very promising results of these nanostructures have been demonstrated. For example, Wang and co-workers [27] have prepared SnO_2 nanoflowers via a one-pot hydrothermal treatment using cetyltrimethylammonium bromide (CTAB) as the soft template, which have exhibited enhanced gas sensing properties for n-butanol. Chen et al. [11] have successfully synthesized SnO_2 nanopolyhedrons assembled by ultrathin SnO_2 nanowires based on the sodium dodecyl sulfate (SDS)-assisted hydrothermal process. Compared with other methods, hydrothermal synthesis has been proven an effective, convenient and economical way to prepare hierarchical nanostructured SnO_2. At the same time, applications of the synthesis hierarchical SnO_2 nanostructures can be expanded by developing a simple template-free hydrothermal method.

In this work, a simple template-free hydrothermal synthesis is used to obtain a 3D flower-shaped SnO_2 self-assembled by SnO_2 nanorods. The crystallinity, morphology and crystal structure of the as-prepared SnO_2 are characterized in detail. Moreover, systematic experiments were performed to understand the formation mechanism of the hierarchical SnO_2 nanostructures. Excellent acetone and ethanol sensing properties of the hierarchical SnO_2 nanoflowers were observed at the operating temperature lower than 200 °C. The result indicates that it is possible for as-prepared

* Corresponding author.
E-mail address: q_wang@cauc.edu.cn (Q. Wang).

http://dx.doi.org/10.1016/j.ceramint.2016.07.062
0272-8842/

SnO_2 nanostructures to be promising applications as the chemical sensor.

2. Experimental section

2.1. Materials and methods

Materials used were all of analytical grade without further purification. In a typical synthesis, $K_2SnO_3 \cdot 3H_2O$ (0.299 g, 1.0 mmol) and $Zn(CH_3COO)_2 \cdot 2H_2O$ (0.219 g, 1.0 mmol) were dissolved in 30 mL of ethanol-deionized water mixture (10 mL ethanol and 20 mL deionized water) and stirred for 10 min, respectively. Then the $K_2SnO_3 \cdot 3H_2O$ solution was added dropwise to the $Zn(CH_3COO)_2 \cdot 2H_2O$ solution and their mixture was stirred for 15 min. After that, the urea (1.8 g, 30 mmol) was dissolved in the above system to obtain a white suspension solution, which was then transferred into a 100 mL Teflon-lined stainless steel autoclave and heated at 180 °C for 24 h. After it cooled down to the room temperature, the white precipitate was washed several times with deionized water and ethanol, and then dried under vacuum at 50 °C overnight. The final product was annealed at 450 °C for 2 h in air.

2.2. Characterization

The morphology and size of the resulting powder were characterized by a field-emission scanning electron microscope (FESEM, JEOL-6701 F, operated at 10 kV) and transmission electron microscopy (TEM, JEOL2010). Powder X-Ray diffraction (XRD) patterns were collected on a Rigaku D/max-2500 with filtered Cu K_α radiation (λ=0.1542 nm) at 40 kV and 100 mA. The nitrogen adsorption and desorption isotherms were measured using a Quantachrome Autosorb AS-1 instrument.

2.3. Sensor fabrication and test

The fabrication procedure of side-heated gas sensor was briefly described typically as our previous study [31]: the as-prepared SnO_2 products were mixed with deionized water at a weight ratio of 2:1 to form a homogeneous paste. Then the paste was coated onto an alumina ceramic tube (size and dimension of about 2.5 × 4.0 mm) to form a thin 20 μm sensing film. The ceramic tube was previously positioned with a pair of Au electrodes and two Pt wires on each end. A Ni–Cr alloy coil was inserted into the tube as a heater to provide the working temperature of the gas sensor by tuning on the heating voltage. Finally, the alumina tube was welded onto a pedestal with six probes.

The electrical properties of the gas sensor were measured by a CGS-8 gas-sensing testing system (Beijing Elite Tech Co. Ltd., PR China). A stationary-state gas distribution process was performed to complete the measurement: a given amount of tested gas was injected into a glass chamber and fully mixed with air. The response of the sensor was defined as the ratio (R_a/R_g) of the resistance of the sensor in air (R_a) to that in a testing gas (R_g). The response and recovery time were defined as the time taken by the sensor to achieve 90% of the total resistance change in the case of adsorption and desorption, respectively.

3. Results and discussion

3.1. Structural and morphological characterization

The phase purity and the crystallographic structure of the as-synthesized products were characterized by X-ray diffraction. The

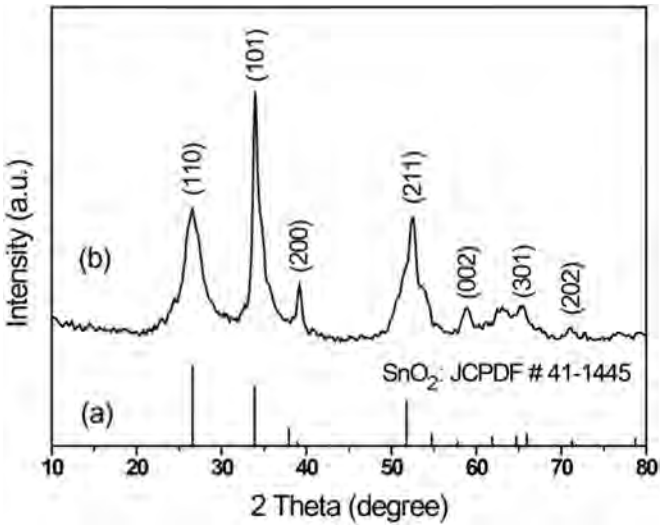

Fig. 1. (a) Standard reflection peaks of rutile SnO_2 (JCPDS card No. 41-1445) and (b) XRD pattern of the as-synthesized SnO_2 products.

XRD patterns of the flower-like SnO_2 are shown in Fig. 1b, where all the diffraction peaks can be indexed to the standard diffraction pattern of rutile SnO_2 (Fig. 1a, JCPDS card No. 41-1445). No other reflection peaks such as ZnO, $ZnSnO_3$, etc., could be observed, indicating the full crystallinity of the obtained SnO_2 products. The formation of nanosized SnO_2 crystals are indicated by the broad peaks, which is confirmed as below.

The size and morphology of the obtained SnO_2 sample were examined by scanning electron microscopy (SEM). The low-magnification SEM image in Fig. 2a shows that the sample almost completely consisted of uniform flower-like structures with an average diameter of about 200 nm. At an enlarged magnification (Fig. 2b), it can be apparently observed that each of the hierarchical nanostructures is composed of tens of similar SnO_2 nanorods with a diameter of about 25 nm and a length of about 80 nm.

The detailed hierarchical structures of the flower-like SnO_2 products are further characterized by transmission electron microscopy (TEM). From the representative low-magnification TEM image of the as-synthesized products (Fig. 3a), it can be seen that well-dispersed nanoflowers with average size around 200 nm are in accordance with the SEM results. The high-magnification TEM image (Fig. 3b) reveals that the flower-like hierarchical nanostructures actually are self-assembled by uniform SnO_2 nanorods with diameter of about 20–25 nm with sharp tips, which is consistent with the broadened XRD patterns. In Fig. 3c, it is apparent that the lattice spacing of 0.335 nm corresponds to the (110) planes of tetragonal rutile SnO_2. Interestingly, it is noteworthy that the hierarchical flower-like nanostructures are sufficiently stable, which cannot be destroyed even after the ultrasonication for 60 min

The nitrogen adsorption-desorption was performed to determine the specific surface areas of as-prepared hierarchical SnO_2 nanoflowers. As shown in Fig. 4, the Brunauer-Emmett-Teller (BET) specific surface area of the sample calculated from N_2 adsorption is 51 m^2/g, and the isotherm of the SnO_2 sample exhibits a hysteresis loop at the P/P_0 ranges of 0.88–0.98, which is associated with the filling and emptying of mesopores by capillary condensation. The pore size distribution of the SnO_2 nanoflowers show that a broad peak appears in the pore size region of 6–120 nm. The larger specific surface area of the SnO_2 can be ascribed to its three-dimensional hierarchical nanostructures. It is well-known that porous nanostructures with large specific surface area as gas sensors

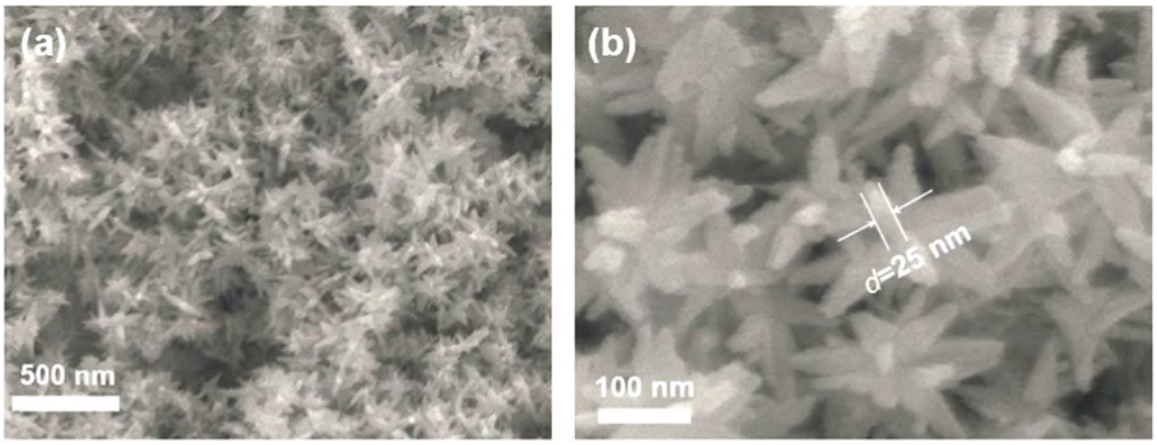

Fig. 2. (a) Low- and (b) high-magnification SEM images of the as-synthesized SnO_2 products.

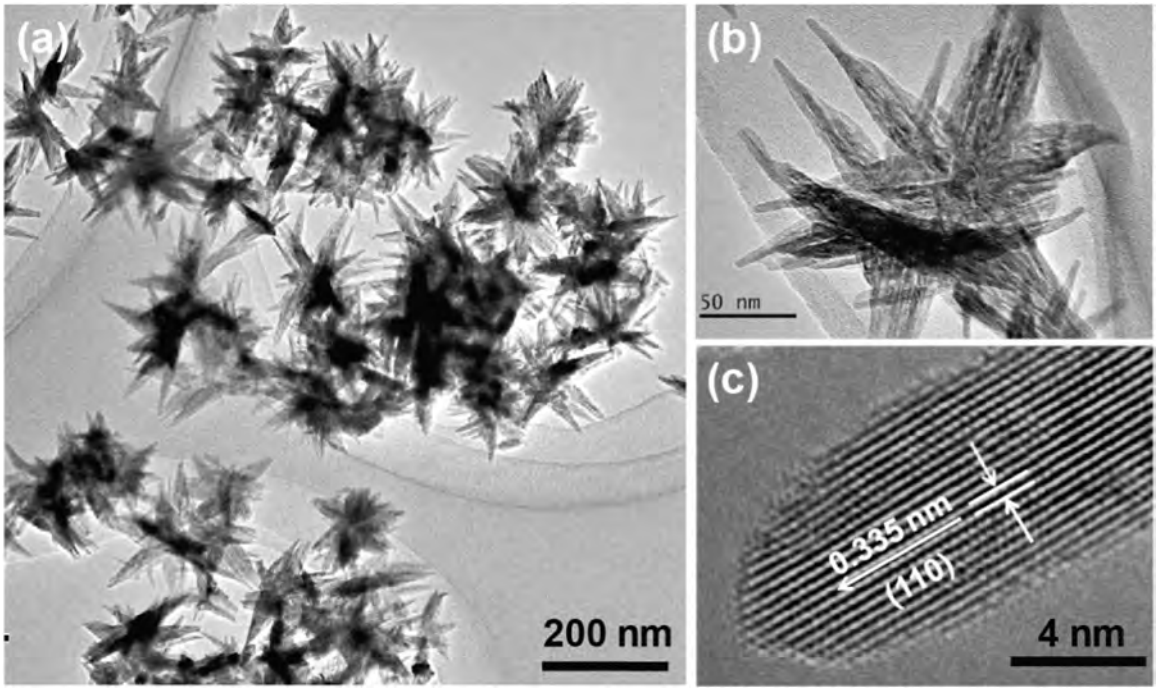

Fig. 3. (a) Low-magnification TEM images of the flower-like SnO_2 products. (b) High-magnification TEM images of individual SnO_2 nanoflower. (c) Lattice-resolved HRTEM image taken from the tip of SnO_2 nanorod.

enable more detected gases to participate in surface reactions, suggesting the potential application of SnO_2 nanoflowers as gas sensors.

3.2. Growth mechanism and formation process

To understand the formation process of the hierarchical SnO_2 nanoflowers and the possible growth mechanism, a series of controllable experiments were also carried out. The composition and morphology of the samples prepared at different reaction times were investigated. Uniform cubic nanostructures with edge size of 80–100 nm can be observed before the hydrothermal treatment in Fig. 5a. The crystallinity and phase information of the cube-like precursors are confirmed by XRD measurements in Fig. 6a. It is indexed to the standard $ZnSn(OH)_6$ phase (JCPDS card No. 20-1455), demonstrating a phase transformation after the hydrothermal reaction. As the hydrothermal process was prolonged to 6 h, the SEM image in Fig. 5b shows a large quantity of nanorods on the surface of $ZnSn(OH)_6$ nanocubes. The diffraction peaks marked "◆" in Fig. 6b can be indexed to tetragonal SnO_2 (JCPDS card No. 41-1445), suggesting that the composites of $ZnSn(OH)_6$ and SnO_2 are obtained. When the reaction time increased to 12 h, 3D SnO_2 nanoflower nanostructures can be assembled by the SnO_2 nanorods. Meanwhile, the amount of $ZnSn(OH)_6$ also decreased and cannot be detected by XRD in Fig. 6c. When the reaction time proceeded to 18 h, it can be seen in Fig. 5d that $ZnSn(OH)_6$ nanocubes completely disappeared and further changed into SnO_2 nanoflowers, which is also illustrated based on the XRD result in Fig. 6d.

On the basis of the time-dependent experiments results, a possible growth mechanism can be proposed in Fig. 7. In the first step, after the mixture of reactants (Zn^{2+} and SnO_3^{2-}) are obtained, H_2SnO_3 and $Zn(OH)_4^{2-}$ are produced to form $ZnSn(OH)_6$ nanocubes (Fig. 5a) due to the dual-hydrolysis-assisted liquid precipitation reaction. Then, with the increase of temperature during the hydrothermal reaction process, urea is hydrolyzed (when the temperature was higher than 60 °C) as follows:

$$(NH_2)_2CO + H_2O \rightarrow 2NH_3 + CO_2 \quad (1)$$

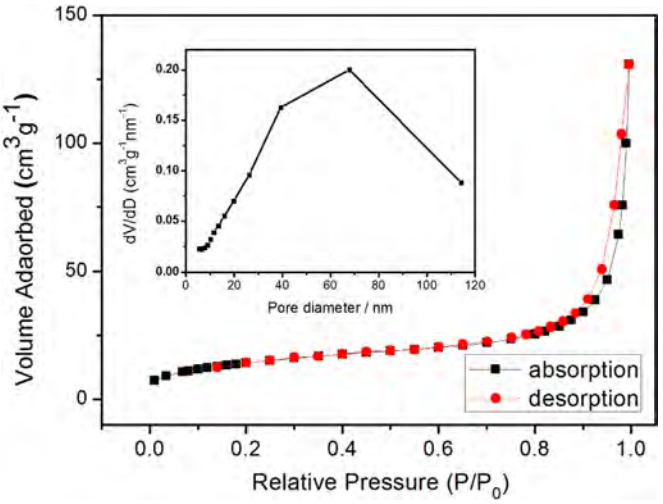

Fig. 4. Typical nitrogen adsorption and desorption isotherms of the SnO_2 nanoflowers with corresponding pore-size distribution (inset) calculated by the BJH method from the desorption branch.

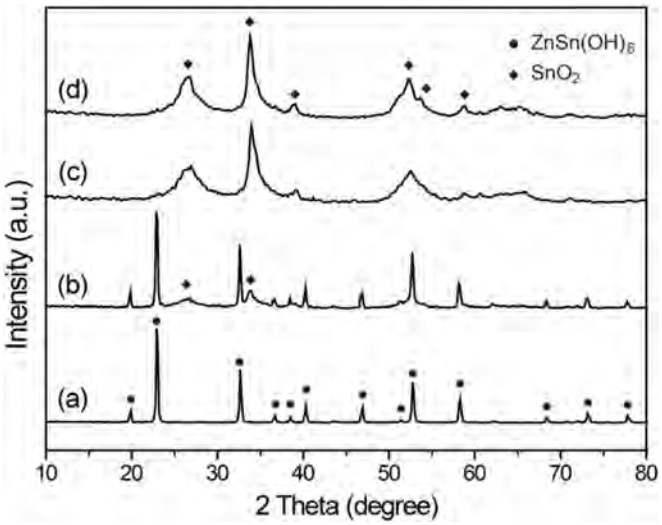

Fig. 6. XRD patterns of the SnO_2 nanostructures prepared with different reaction times: (a) 0 h, (b) 6 h, (c) 12 h, (d) 18 h.

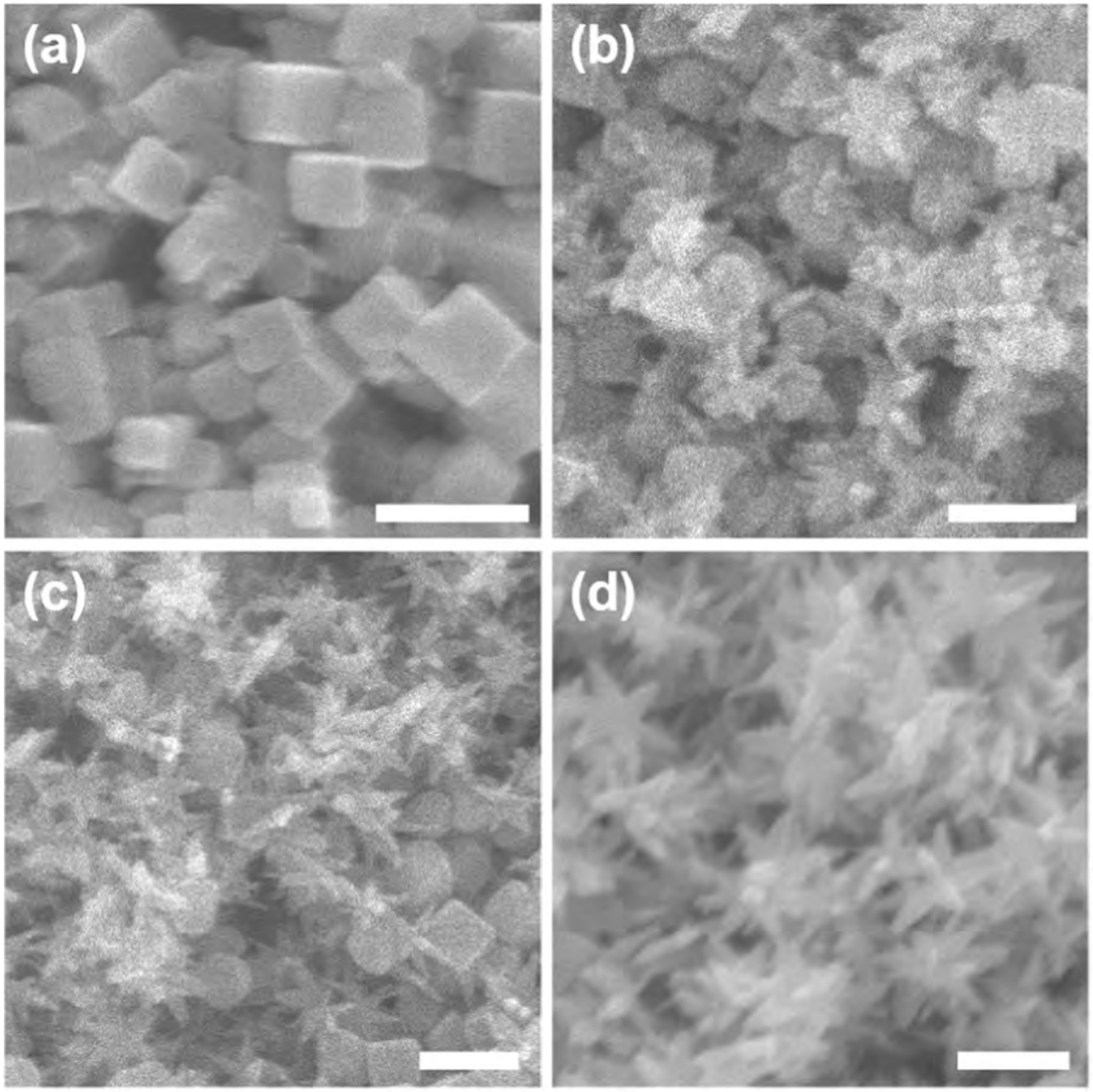

Fig. 5. SEM images of morphology evolution of the SnO_2 nanostructures prepared with different reaction times: (a) 0 h, (b) 6 h, (c) 12 h, (d) 18 h. The scale bar is 200 nm.

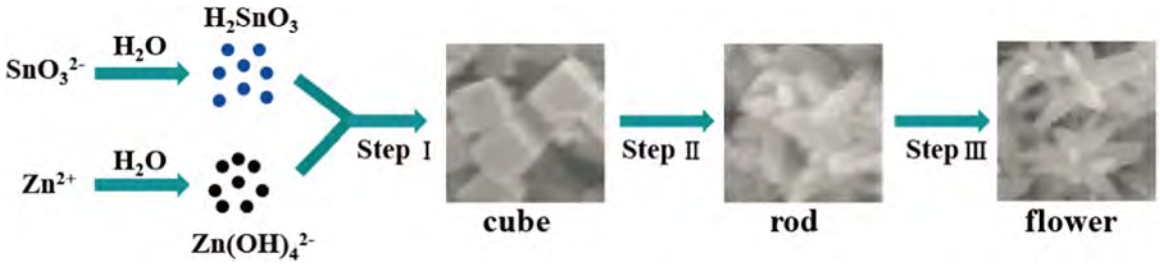

Fig. 7. Schematic illustration of the transformation process of SnO_2 nanoflowers.

Interestingly, under the hydrothermal reaction system, $Zn(OH)_6$ is dissolved by NH_3, which lead to the formation a soluble complex $Zn(NH_3)_4^{2+}$ kept in the mother solution. Meanwhile, SnO_2 was easily formed by the Sn^{4+} ions at basic conditions [32,33]. Chemical reaction process of SnO_2 can be formulated as follows:

$$ZnSn(OH)_6 + 4NH_3 \rightarrow SnO_2 + [Zn(NH_3)_4]^{2+} + 2OH^- + 2H_2O \quad (2)$$

According to the previous reports, SnO_2 (001) crystal exhibits the highest surface energies, and it is more favorable for crystal to grow along the (001) direction so that SnO_2 nanorods can be obtained [34–36]. Obviously, in this reaction system, urea molecules also played an important role in the formation of SnO_2 nanoflowers. As the reaction proceeded, more NH_3 were produced, thus resulting in more SnO_2 primary nanorods. Finally, in the step III, the hierarchical SnO_2 nanoflowers with many rod-like structures were obtained through a self-assembled process. The detailed mechanism of the self-assemble process is still under investigation by our group.

3.3. Gas sensing properties

A sensor based on the as-synthesized SnO_2 nanoflowers was developed and tested by a method similar to that in our previous reports [31]. As shown in Fig. 8a, in order to determine the optimal working temperature of the sensor based on the SnO_2 nanoflowers, the gas sensing responses values of the sensor to 50 ppm acetone and ethanol were investigated at the working temperature in the range of 120–300 °C. It can be seen that the optimal working temperatures of gas sensors to acetone and ethanol are 170 °C and 200 °C, and the maximum responses to 50 ppm acetone and 50 ppm ethanol reach 29.2 and 21.1, respectively. The difference in the working temperature can be attributed to the different activation energy barriers related to different sensing gases [37]. In general, the SnO_2 sensors are usually operated at relatively high temperature of 300–500 °C [38–40], which is not favorable in many practical fields. In addition to loading noble metals (e.g. Pt, Pd, Au, and Ag) on the surface of SnO_2, reduction of the grain size of SnO_2 is also an available approach to lower the sensor's working temperature. In Fig. 3b and c, it can be clearly seen that the diameter of the SnO_2 sample tips is less than 2 L (about 6 nm), where L is the depth of the space-charge layer, thus the response and operating temperature can be greatly influenced [41–43].

Selectivity is an important parameter of gas sensors and indicates the response ability of a sensor to a certain gas in presence of other gases. As shown in Fig. 8b, the sensing selectivity of the SnO_2 nanoflowers sensor is also investigated, and the gas response towards ethanol, acetone, methanol, toluene and chloroform with concentration 50 ppm each at 170 °C and 200 °C are compared, respectively. It is found that the SnO_2 nanoflowers-based gas sensor exhibits high response ability to acetone and ethanol. Interestingly, its response to acetone is obvious, reaching a maximum value of 29.2 but no higher than 10 to other gases at 170 °C. The results indicates a preferable selectivity of the SnO_2 nanoflowers-based sensor in the detection of acetone.

Fig. 9 shows the real-time response curves and the sensor responses of the SnO_2 nanoflowers sensor device upon exposure to different concentrations of acetone and ethanol at a working temperature of 170 °C and 200 °C, respectively. It can been see that the response value of the sensor increases quickly with the injection of tested gases while decreases rapidly and recovers to its initial value with the release of tested gases. Furthermore, with increasing concentration at their optimal operating temperatures, the obtained gas sensor presented sensitive and reversible responses to both acetone and ethanol. As shown in Fig. 9a and c, the sensor exhibits a lower response ability to ethanol gas from 5 to 200 ppm compared with that to acetone gas, with the response

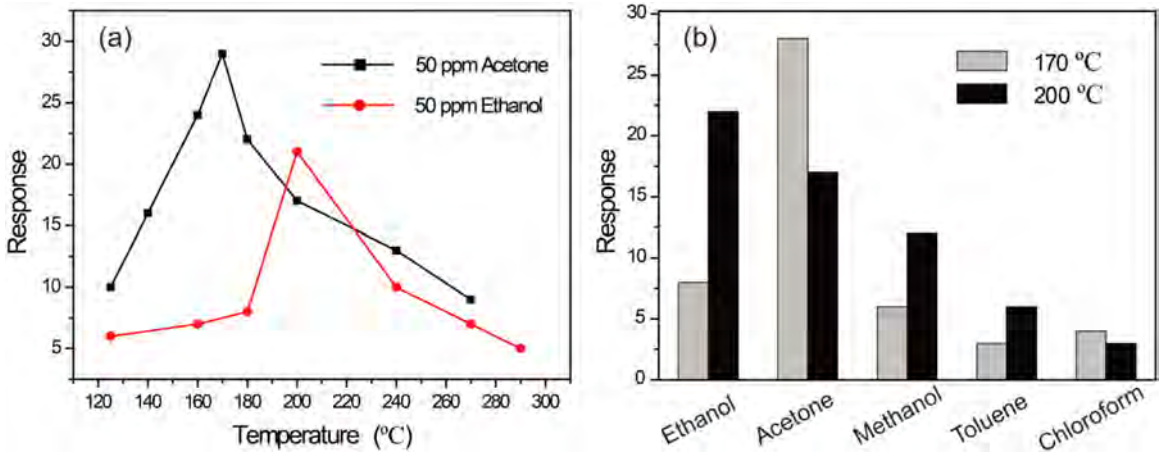

Fig. 8. (a) Gas sensing responses values of as-fabricated gas sensors with different working temperatures in 50 ppm acetone and ethanol, respectively. (b) The plots of the response of the sensors based on the SnO_2 nanoflowers with different gases with a concentration of 50 ppm at 170 °C (gray) and 200 °C (black), respectively.

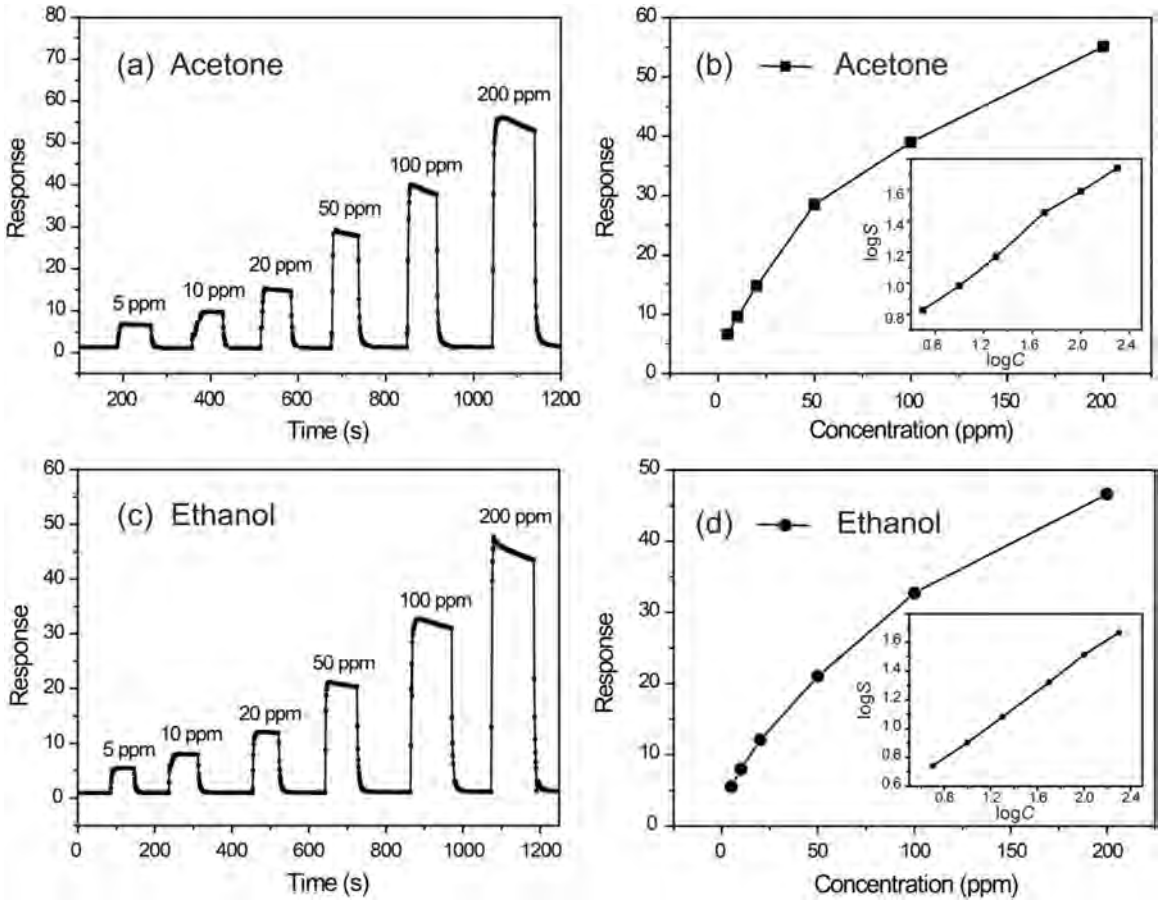

Fig. 9. Real-time response curves and sensor responses of the SnO_2 nanoflowers sensor to different concentrations of acetone (a and b), ethanol (c and d) at a working temperature of 170 °C and 200 °C, respectively. Logarithm plots of the acetone sensor (inset of Fig. 9b) and ethanol sensor (inset of Fig. 9d) on response value versus the gas concentration (5–200 ppm).

values of 5.5, 8, 12, 21, 32 and 46 to 5, 10, 20, 50, 100, 200 ppm ethanol gas versus the response values of 6.5, 9.5, 15, 29, 39 and 55 to 5, 10, 20, 50, 100, 200 ppm acetone gas. When the concentration of tested gases (acetone and ethanol) is in the range of 5–200 ppm, the logarithm of the sensor response exhibits good linearity with that of the tested gas concentration (as shown in the inset of Fig. 9b and d).

Response and recovery times are also important parameters of a gas sensor. The response and recovery time were defined as the time taken by the sensor to achieve 90% of the total resistance change in the case of adsorption and desorption, respectively. In Fig. 10, it can been clearly seen that the response and recovery time of the SnO_2 nanoflowers sensor in 20 ppm acetone are 3 and 30 s (Fig. 10a), whereas the response and recovery times are 4 and 22 s when exposed to 20 ppm ethanol (Fig. 10b), suggesting the good response and recovery properties of the sensor. Table 1 shows the acetone-sensing properties of SnO^{2-} based gas sensors. As shown in the Table 1, the as-synthesized SnO_2 nanoflowers exhibit good gas-sensing performance, especially at a low operating temperature among those have been reported up to now.

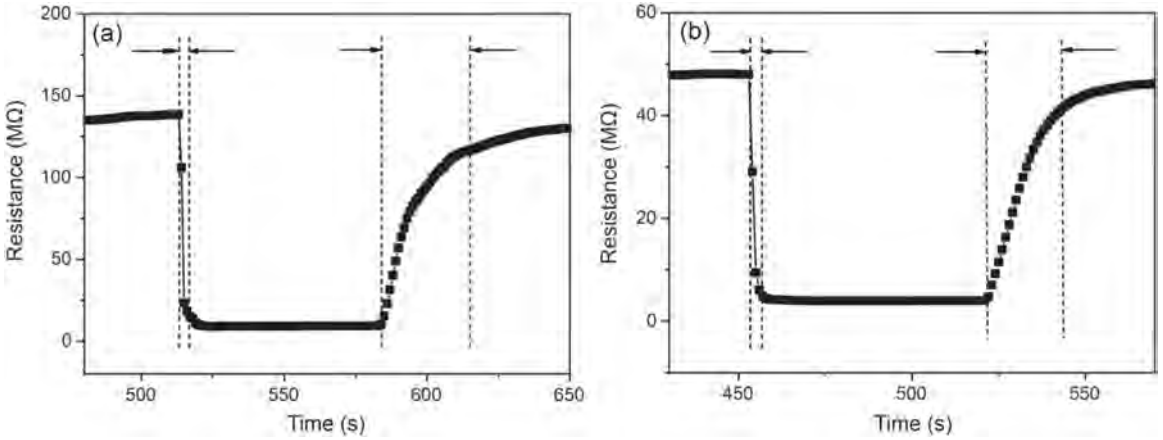

Fig. 10. Response-recovery curves of the SnO_2 nanoflowers in 20 ppm (a) acetone and (b) ethanol at a working temperature of 170 °C and 200 °C, respectively.

Table 1
Comparison between SnO_2 nanoflowers and other SnO_2 nanostructures reported in the literatures.

Materials	Temperature (°C)	Acetone concentration	Sensor response	Response-recovery time (s)	Reference
SnO_2 nanopolyhedrons	370	200 ppm	48	9.7/5.8	[5]
SnO_2 nanospike arrays	320	200 ppm	65	5/23	[24]
SnO_2 hollow nanospheres	400	100 ppm	8.5	17/19	[15]
SnO_2 nanosheets	310	100 ppm	9.8	3.6/19	[25]
SnO_2 hollow nanosheets	300	50 ppm	18.3	0.9/5.8	[30]
SnO_2 nanoflowers	170	50 ppm	29.2	3/28	This work

3.4. Sensing mechanism

As a typical n-type semiconductor oxide, the gas-sensing mechanism for SnO_2 gas sensors belongs to the surface-resistance controlled model. In general, gas sensing on the surface of SnO_2 is an adsorption-desorption process that leads to a change in the electrical resistance of the sensing material. At the working temperature in air, the oxygen will be adsorbed on the SnO_2 surfaces. The electrons from the conduction band of SnO_2 can be captured by those oxygen molecules, which leads to the formation of chemically-adsorbed oxygenate species, such as O^{2-}, O^- and O_2^-. As a result, the resistance of SnO_2 reaches the highest level. With the reaction between oxygenate species and reductive gases, such as acetone and ethanol, electrons are then released to SnO_2 surfaces, resulting in a dramatic decrease of the resistance of SnO_2. This redox progress can be described by the following equations:

$$O_2(gas) \rightarrow O_2(ads) \quad (3)$$

$$O_2(ads) + e^- \rightarrow O^-(O_2^-, O^{2-})(ads) \quad (4)$$

$$C_2H_5OH + 6O^-(O_2^-, O^{2-})(ads) \rightarrow 2CO_2 + 3H_2O + 6e^- \quad (5)$$

$$CH_3COCH_3 + 8O^-(O_2^-, O^{2-})(ads) \rightarrow 3CO_2 + 3H_2O + 8e^- \quad (6)$$

The capability to adsorb oxygen molecules in air is crucial to improve the gas sensing performance. It is apparent that the gas sensing properties of SnO_2 are also influenced by its crystalline size and surface modification besides microstructure. As shown in Fig. 4, the BET specific surface area of the SnO_2 nanoflowers calculated from N_2 adsorption is 51 m^2/g, which is much larger than that of the commercial SnO_2 samples. Larger specific surface area is adopted to provide more chance for oxygen molecules to be absorbed on the surface of the SnO_2 sensor in air, and for free electrons from the conduction band to participate in the formation of chemisorbed oxygen species (O^{2-}, O^- and O_2^-). Furthermore, the enhancement in gas-sensing properties on the nanoflower SnO_2 sensor, including high response and fast response-recovery ability, are also attributed to the unique 3D hierarchical nanostructure, which can significantly facilitate gas diffusion and mass transportation in the sensing materials. Besides the large specific surface area and the nanoflower structure, it is generally considered that the presence of SnO_2 nanorods as building blocks can be an important reason to improve the gas-sensing performance. In Fig. 3b and c, it is apparent that the diameter of the SnO_2 sample tips is less than $2L$ ($L=3$ nm, thickness of the depletion layer), and that the 1D materials is also the smallest dimension structure to transport electrons more efficiently than other morphologies, so that the response and operating temperature can be greatly influenced.

4. Conclusions

In summary, nanorod self-assembled 3D SnO_2 flower-like nanostructures with size about 200 nm have been successfully synthesized by a one-pot hydrothermal synthesis process without any templates and surfactants in the reaction system, and as-synthesized products have been nearly monodispersed and aggregated by the assembly of SnO_2 nanorod with length and diameter of about 80 nm and 25 nm, respectively. According to the morphology and crystal structure on the evolution of hierarchical SnO_2, a possible formation mechanism is proposed base on the observation of precipitation-hydrolysis-nucleation and self-assembly of 1D SnO_2 nanorods as building blocks. When evaluated as the potential application in gas sensing materials, the SnO_2 nanoflower architectures exhibits high response and fast response-recovery ability to acetone and ethanol at a working temperature lower than 200 °C. The 3D hierarchical SnO_2 nanostructures are also excepted to be applicable in other fields such as lithium-ion batteries, catalysis and dye-sensitized solar cells.

Acknowledgments

The project was mainly supported by the Fundamental Research Funds for the Central Universities (3122013k007), the Applied Basic and Cutting-edge Research Programs of Science and Technology Foundation of Tianjin (No. 13JCQNJC07100), the National College Students' Innovation Entrepreneurial Training Project IECAUC201510059045), the National Natural Science Foundation of China (21501196), the Science and Technology Innovation Project 2015 of Civil Aviation Administration of China–Study on Airworthiness Certification Technology of Large Aircraft Cabin Air Environment (MHRD20150220) and the Science and Technology Innovation Guide Funds of Civil Aviation Administration of China (2014), is supplemented as (MHRD20140209).

References

[1] Y. Xia, P. Yang, Y. Sun, Y. Wu, B. Mayers, B. Gates, Y. Yin, F. Kim, H. Yan, One-dimensional nanostructures: synthesis, characterization, and applications, Adv. Mater. 15 (2003) 353–389.
[2] G. Shen, J. Xu, X. Wang, H. Huang, D. Chen, Growth of directly transferable In_2O_3 manowire mats for transparent thin-film transistor applications, Adv. Mater. 23 (2011) 771–775.
[3] Y. Sun, S. Gao, Y. Xie, Atomically-thick two-dimensional crystals: electronic structure regulation and energy device construction, Chem. Soc. Rev. 43 (2014) 530–546.
[4] G. Chen, Z. Liu, B. Liang, G. Yu, Z. Xie, H. Huang, B. Liu, X. Wang, D. Chen, M.-Q. Zhu, G. Shen, Single-crystalline p-Type Zn_3As_2 nanowires for field-effect transistors and visible-light photodetectors on rigid and flexible substrates, Adv. Funct. Mater. 23 (2013) 2681–2690.
[5] X. Zhang, L. Yang, Y. Jiang, B.-B. Yu, Y.-G. Zou, Y. Fang, J.-S. Hu, L.-J. Wan, Facile solution synthesis and photoelectric properties of monolithic tin(II) sulfide nanobelt arrays, Chemistry – Asian J. 8 (2013) 2483–2488.
[6] D. Chen, J. Xu, B. Liang, X.-F. Wang, P.-C. Chen, C.-W. Zhou, G.-Z. Shen, Electric transport, reversible wettability and chemical sensing of single-crystalline zigzag Zn_2SnO_4 nanowires, J. Mater. Chem. 21 (2011) 17236–17241.
[7] B. Gong, Z. Shao, Self-assembling organic nanotubes with precisely defined, sub-nanometer pores: formation and mass transport characteristics, Acc. Chem. Res. 46 (2013) 2856–2866.
[8] H.-J. Kim, T. Kim, M. Lee, Responsive nanostructures from aqueous assembly of rigid – flexible block molecules, Acc. Chem. Res. 44 (2010) 72–82.
[9] G. Shen, D. Chen, Self-coiling of $Ag_2V_4O_{11}$ nanobelts into perfect nanorings and

microloops, J. Am. Chem. Soc. 128 (2006) 11762–11763.
[10] H. Shi, L. Qi, J. Ma, H. Cheng, Polymer-directed synthesis of penniform $BaWO_4$ nanostructures in reverse Micelles, J. Am. Chem. Soc. 125 (2003) 3450–3451.
[11] D. Chen, J. Xu, Z. Xie, G. Shen, Nanowires assembled SnO_2 nanopolyhedrons with enhanced gas sensing properties, ACS Appl. Mater. Inter 3 (2011) 2112–2117.
[12] M. Chang, X.L. Cao, H. Zeng, L. Zhang, Enhancement of the ultraviolet emission of ZnO nanostructures by polyaniline modification, Chem. Phys. Lett. 446 (2007) 370–373.
[13] D. Kim, H.C. Park, K.-H. Lee, K.-B. Park, K. Choi, W. Hwang, Overcoming of nanoscale adhesion by electrostatic induction, Curr. Appl. Phys. 9 (2009) 703–706.
[14] H. Wang, A.L. Rogach, Hierarchical SnO_2 nanostructures: recent advances in design, synthesis, and applications, Chem. Mater. 26 (2014) 123–133.
[15] X. Ma, H. Song, C. Guan, Interfacial oxidation–dehydration induced formation of porous SnO_2 hollow nanospheres and their gas sensing properties, Sens. Actuators B-Chemical 177 (2013) 196–204.
[16] A.A. Firooz, A.R. Mahjoub, A.A. Khodadadi, Highly sensitive CO and ethanol nanoflower-like SnO_2 sensor among various morphologies obtained by using single and mixed ionic surfactant templates, Sens. Actuators B-Chemical 141 (2009) 89–96.
[17] R. Yang, Y. Gu, Y. Li, J. Zheng, X. Li, Self-assembled 3-D flower-shaped SnO_2 nanostructures with improved electrochemical performance for lithium storage, Acta Mater. 58 (2010) 866–874.
[18] S.H. Mohamed, SnO_2 dendrites–nanowires for optoelectronic and gas sensing applications, J. Alloy. Compd. 510 (2012) 119–124.
[19] S. Liu, M. Xie, Y. Li, X. Guo, W. Ji, W. Ding, C. Au, Novel sea urchin-like hollow core–shell SnO_2 superstructures: Facile synthesis and excellent ethanol sensing performance, Sens. Actuators B-Chemical 151 (2010) 229–235.
[20] X.-G. Han, S.-F. Xie, Q. Kuang, Z.-Y. Jiang, Y.-Q. Jiang, Z.-X. Xie, L.-S. Zheng, Synthesis of tin dioxide octahedral nanoparticles with exposed high-energy {221} facets and enhanced gas-sensing properties, Angew. Chem. Int. Ed. 48 (2009) 9180–9183.
[21] T. Kida, Doi Takayuki, Shimanoe Kengo, Synthesis of monodispersed SnO_2 nanocrystals and their remarkably high sensitivity to volatile organic compounds, Chem. Mater. 22 (2010) 2662–2667.
[22] L.-Y. Jiang, X.-L. Wu, Y.-G. Guo, L.-J. Wan, SnO_2-based hierarchical nanomicrostructures: facile synthesis and their applications in gas sensors and lithium-ion batteries, J. Phys. Chem. C 113 (2009) 14213–14219.
[23] Y. Wang, X. Jiang, Y. Xia, A solution-phase, precursor route to polycrystalline SnO_2 nanowires that can be used for gas sensing under ambient conditions, J. Am. Chem. Soc. 125 (2003) 16176–16177.
[24] J. Xu, Y. Li, H. Huang, Y. Zhu, Z. Wang, Z. Xie, X. Wang, D. Chen, G. Shen, Synthesis, characterizations and improved gas-sensing performance of SnO_2 nanospike arrays, J. Mater. Chem. 21 (2011) 19086–19092.
[25] H. Chen, Q. Wang, C. Kou, Y. Sui, Y. Zeng, F. Du, One-pot synthesis and improved sensing properties of hierarchical flowerlike SnO_2 assembled from sheet and ultra-thin rod subunits, Sens. Actuators B-Chemical 194 (2014) 447–453.
[26] J. Huang, X. Xu, C. Gu, S. Yao, Y. Sun, J. Liu, Large-scale selective preparation of porous SnO_2 3D architectures and their gas-sensing property, CrystEngComm 14 (2012) 3283–3290.
[27] L. Wang, S. Wang, Y. Wang, H. Zhang, Y. Kang, W. Huang, Synthesis of hierarchical SnO_2 nanostructures assembled with nanosheets and their improved gas sensing properties, Sens. Actuators B-Chemical 188 (2013) 85–93.
[28] H. Wang, Q. Liang, W. Wang, Y. An, J. Li, L. Guo, Preparation of flower-like SnO_2 nanostructures and their applications in gas-sensing and lithium storage, Cryst. Growth Des. 11 (2011) 2942–2947.
[29] L. Zhang, Y. Yin, Hierarchically mesoporous SnO_2 nanosheets: hydrothermal synthesis and highly ethanol-sensitive properties operated at low temperature, Sens. Actuators, B-Chemical 185 (2013) 594–601.
[30] Y. Zeng, Y. Wang, L. Qiao, Y. Bing, B. Zou, W. Zheng, Synthesis and the improved sensing properties of hierarchical SnO_2 hollow nanosheets with mesoporous and multilayered interiors, Sens. Actuators, B-Chemical 222 (2016) 354–361.
[31] D. An, Q. Wang, X. Tong, Q. Zhou, Z. Li, Y. Zou, X. Lian, Y. Li, Synthesis of Zn_2SnO_4 via a co-precipitation method and its gas-sensing property toward ethanol, Sens. Actuators B-Chemical 213 (2015) 155–163.
[32] V. Juttukonda, R.L. Paddock, J.E. Raymond, D. Denomme, A.E. Richardson, L. E. Slusher, B.D. Fahlman, Facile synthesis of tin oxide nanoparticles stabilized by dendritic polymers, J. Am. Chem. Soc. 128 (2006) 420–421.
[33] J. Yin, X. Wang, R. Li, G. Wang, W. Zhang, Synthesis and characterization of hierarchical SnO_2 hollow octahedra, Mater. Lett. 113 (2013) 118–121.
[34] B. Cheng, J.M. Russell, Shi, L. Zhang, E.T. Samulski, Large-scale, solution-phase growth of single-crystalline SnO_2 nanorods, J. Am. Chem. Soc. 126 (2004) 5972–5973.
[35] L. Vayssieres, M. Graetzel, Highly ordered SnO_2 nanorod arrays from controlled aqueous growth, Angew. Chem. Int. Ed. 43 (2004) 3666–3670.
[36] J. Xu, D. Wang, L. Qin, W. Yu, Q. Pan, SnO_2 nanorods and hollow spheres: Controlled synthesis and gas sensing properties, Sens. Actuators B-Chemical 137 (2009) 490–495.
[37] Y.S. Kim, S.-C. Ha, K. Kim, H. Yang, S.-Y. Choi, Y.T. Kim, J.T. Park, C.H. Lee, J. Choi, J. Paek, K. Lee, Room-temperature semiconductor gas sensor based on nonstoichiometric tungsten oxide nanorod film, Appl. Phys. Lett. 86 (2005) 213105.
[38] L.-S. Zhang, L.-Y. Jiang, C.-Q. Chen, W. Li, W.-G. Song, Y.-G. Guo, Programmed fabrication of metal oxides nanostructures using dual templates to spatially disperse metal oxide nanocrystals, Chem. Mater. 22 (2009) 414–419.
[39] M. Tiemann, Porous metal oxides as gas sensors, Chemistry – Eur. J. 13 (2007) 8376–8388.
[40] J.-H. Lee, Gas sensors using hierarchical and hollow oxide nanostructures: overview, Sens. Actuators B-Chemical 140 (2009) 319–336.
[41] Y. Jia, L. He, Z. Guo, X. Chen, F. Meng, T. Luo, M. Li, J. Liu, Preparation of porous tin oxide nanotubes using carbon nanotubes as templates and their gas-sensing properties, J. Phys. Chem. C 113 (2009) 9581–9587.
[42] H. Hui, Y.C. Lee, O.K. Tan, W. Zhou, N. Peng, Q. Zhang, High sensitivity SnO_2 single-nanorod sensors for the detection of H_2 gas at low temperature, Nanotechnology 20 (2009) 115501.
[43] A. Biaggi-Labiosa, F. Solá, M. Lebrón-Colón, L.J. Evans, J.C. Xu, G.W. Hunter, G. M. Berger, J.M. González, A novel methane sensor based on porous SnO_2 nanorods: room temperature to high temperature detection, Nanotechnology 23 (2012) 455501.